Nanoscale

Accepted Manuscript

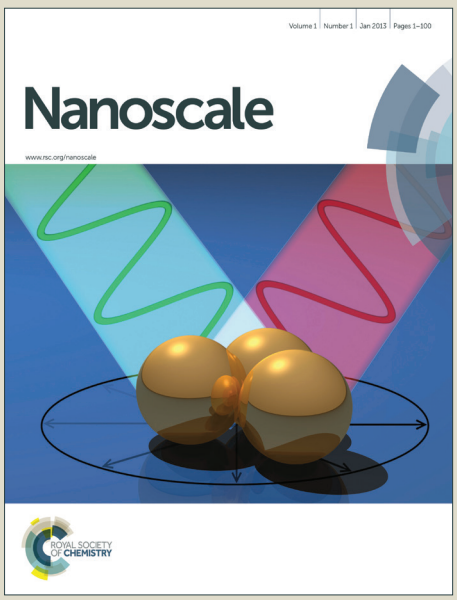

This is an *Accepted Manuscript*, which has been through the Royal Society of Chemistry peer review process and has been accepted for publication.

Accepted Manuscripts are published online shortly after acceptance, before technical editing, formatting and proof reading. Using this free service, authors can make their results available to the community, in citable form, before we publish the edited article. We will replace this *Accepted Manuscript* with the edited and formatted *Advance Article* as soon as it is available.

You can find more information about *Accepted Manuscripts* in the Information for Authors.

Please note that technical editing may introduce minor changes to the text and/or graphics, which may alter content. The journal's standard Terms & Conditions and the Ethical guidelines still apply. In no event shall the Royal Society of Chemistry be held responsible for any errors or omissions in this *Accepted Manuscript* or any consequences arising from the use of any information it contains.

ROYAL SOCIETY OF CHEMISTRY

www.rsc.org/nanoscale

Cite this: DOI: 10.1039/c0xx00000x

www.rsc.org/xxxxxx

ARTICLE TYPE

Si Nanoparticles Encapsulated in Elastic Hollow Carbon Fibre for Li-Ion Battery Anodes with High Structure Stability

*Shan Fang, Laifa Shen, Zhenkun Tong, Hao Zheng, Fang Zhang, Xiaogang Zhang**

Received (in XXX, XXX) Xth XXXXXXXXX 20XX, Accepted Xth XXXXXXXXX 20XX

DOI: 10.1039/b000000x

Silicon has a large specific capacity which is an order of magnitude beyond that of conventional graphite, making it a promising anode material for lithium ion batteries. However, the large volume changes (~300%) during cycling caused material pulverization and instability of the solid-electrolyte interphase resulting in poor cyclability which prevented its commercial application. Here, we have prepared a novel one-dimensional core-shell nanostructure in which the Si nanoparticles have been confined within hollow carbon nanofibres. Such a unique nanostructures exhibits high conductivity, facile ion transport, and the uniform pores within the particles which are generated during magnesiothermic reduction can serve as a buffer zone to accommodate the large volume changes of Si during electrochemical lithiation. Owing to these advantages, the composite shows high rate performance and good cycling stability. The optimum design of the core-shell nanostructure shows promise for the synthesis of a variety of high-performance electrode materials.

Introduction

To meet the great need for high-energy storage for applications in grid energy storage and electric vehicles, much attention has been paid to lithium ion batteries (LIBs) because of their relatively high energy and power densities as well as their lower cost.[1-4] The current carbonaceous anode materials are far from meeting these requirements due to their low theoretical capacity of 372 mAh g^{-1}.[5] Thus, research efforts are devoted to the search for applicable electrode materials with higher energy densities, stable cycle life, and higher rate capacity. Silicon, as a candidate anode material for next generation LIBs, has an unparalleled theoretical capacity of 4200 mAh g^{-1} (in the form of $Li_{4.4}Si$),[6-8] which is about ten times that of commercially available graphite anodes. Additionally, Si is abundant and environmentally benign. However, Si-based electrodes commonly suffer from rapid capacity fade and significant capacity degradation in their early cycles. This stems from the Si anodes which inevitably experience large volume metric strain (both expansion and contraction, of about 300%) due to Li insertion and extraction during charge/discharge cycles: this often results in its structural collapse, active material pulverization, and instability of the solid-electrolyte inter-phase (SEI).[9-11]

Various strategies have been used to alleviate the consequences of volume change.[12-15] For example, Yu's group reported a 3D macroporous silicon particles modified by Ag particles using a facile magnesiothermic reduction and Ag-mirror reaction. The macropores act as interconnected buffer cushions to alleviate the volume change during lithiation/delithiation and the Ag modification also increases the surface electrical conductivity, enhancing the structural stability of the Ag-coated 3D macroporous Si.[14] It has been proved that the electrochemical performance of Si-based electrodes can be improved through three basic strategies: reducing the alloy particle size, using silicon composites, and introducing porous silicon structures.[16-18] There have been reports that Si nanowires,[19, 20] Si nanotubes[21-23], and Si nanoparticles[24, 25] encapsulated in hollow carbon materials are used for nano-engineered active materials. Electro-spinning processes have been used for large applications since a large quantity of one-dimensional nanostructures can be fabricated with fine control of composition and diameter.[9, 26-30] For example, Zhou and co-workers fabricated Si-based materials by encapsulating Si nanoparticles in porous carbon nanofibres by the use of a single-nozzle electro-spinning technique combined with calcination and an etching process.[31] Zhang's group designed a vacant Si@CNF@C composite by electro-spinning and chemical vapour deposition (CVD) technique.[32] They all exhibit good rate capabilities and remarkable cycling stability. While, both of them use SiO_2 as a sacrificial template etched with HF to form a porous structure, and Si nanoparticles mixed with polymer, as electro-spinning solutions. Thus, the Si nanoparticles (Si NPs) cannot be homogeneously distributed within the fibres and are thus easily peeled off.

Considering the aforementioned issues, an optimum design of an exquisite structure was conceived to promote the electrochemical performance of Si-based electrodes, in which Si nanoparticles encapsulated in carbon nanofibres by a facile electrostatic spinning method, surface polymerisation, and an in-situ magnesiothermic reduction reaction were used. In the final product, the carbon fibre is full of Si NPs, which promises a sufficient silicon loading and a high use of the active material. Besides that, the carbon fibres not only enhance the rate capability of the composite electrode but also act as a physical barrier to stabilise the cycle life. This novel structure resolved all of the aforementioned pivotal issues for good Si-based battery operations and indeed showed excellent electrochemical performance.

Experiment Section

Nanoscale Accepted Manuscript

Materials synthesis

Synthesis of SiO_2 nanofibres: SiO_2 nanofibres were synthesized according to the previous literature.[37] In brief, 1.5 g tetraethylorthosilicate (TEOS), 3.5 g absolute ethanol, 4.0 g deionized water (DI) and 1.0 g polyvinylpyrrolidone (PVP) were mixed together and stirred for 1h, until the PVP was dissolved completely, then added 1.0 g of acetic acid in the solution to adjust the samples viscosity. After that, the polymer blend solution was electrospun using conventional electro-spinning equipment. The flow rate of the solutions was 3.5 μL/min. Applied a high voltage of 15 kV, and the distance between the needle and the collector was 9 cm. The as-electrospun fibres were peeled off from the collector and then the sample was transferred into an alumina tube furnace for stabilization and annealed in air at 600 °C for 5 h.

Synthesis of Si NP@C core-shell nanofibres: Typically, 0.5 g SiO_2 nanofibres mixed with dopamine (mass ratio 1:1) were added to the 60 mL of tris-buffer (pH= 8.5) and stirred for 24 h at room temperature. The SiO_2@PDA products were collected by centrifugation and drying in a vacuum oven at 70 °C for a night. The SiO_2@PDA was first carbonized under an N_2 atmosphere at 400 °C for 2 h and 800 °C for 3 h. After that mixed homogeneous with the same amount of magnesium powder, then calcined at temperature of 680 ° C for 6 h under Ar atmosphere. In order to selectively remove MgO, the obtained powder was then dipped into 1 mol L^{-1} HCl solution stirred for 5 h following by washed with DI water and dried at 70 °C for a night. The bare Si nanofibres were synthesized by direct magnesiothermic reduction of SiO_2 nanofibers at 680 °C for 6 h, according to the same preparation procedure for Si NP@C core-shell nanofibres. The capacity was calculated on the total mass of the Si NP@C composite.

Materials Characterization

The crystal structures of the obtained samples were characterized by X-ray diffraction (XRD) (Bruker D8 advance) with Cu K radiation. The mircostructural of the samples were characterized by transmission electron microscopy (TEM, JEOL JEM-2010), scanning electron microscopy (SEM, HITACHI S-4800) and energy-dispersive X-ray spectroscopy (EDX, Phoenix), the nitrogen adsorption/desorption were characterized by Brunauer-Emmett-Teller (BET) measurements using an ASAP-2010 surface area analyzer. Thermogravimetric analyses were carried out on a TG instrument (NETZSCH STA 409 PC) using a heating rate of 5 °C min^{-1} in air from 30 °C to 900 °C.

Electrochemical Test

Electrochemical characterizations were performed by galvanostatic charge/discharge in a coin type cell. The mass ration of samples, carbon black and sodium alginate (Alg) binder is 7:2:1, which mixed and dissolved in DI water, the slurry was uniformly coated on a foil copper current collector used as a working electrode. After that, the electrodes were dried in a vacuum oven at 110 °C for 12 h. The mass of active material loaded on electrode was about 0.7 mg. The cells were assembled in an Ar filled glovebox with Li metal as the counter electrode and the polypropylene film separator. 1 M $LiPF_6$ solution in a mixture of dimethyl carbonate (DMC) and ethylene carbonate (EC) (1:1, by volume) contained 2% (V) fluoroethylene carbonate (FEC) as an electrolyte solution. Galvanostatically charge/discharge experiments were tested using a CT2001A cell test instrument (LAND Electronic Co.) at the potential between 0.01 and 1.5 V (vs. Li/Li^+), the amplitude is 5 mV.

Results and Discussions

Figure 1 shows the experimental procedures: the core–shell structure in the 1D fibres were fabricated by electro-spinning method, surface polymerisation, and magnesiothermic reduction. Briefly, continuous SiO_2 nanofibres were produced by electro-spinning and the original SiO_2 nanofibres were white (see Figure S1a, Supporting Information). Then the SiO_2 nanofibres were directly used as a template and silicon resource. The carbon coating was obtained by using self-polymerising dopamine on the surface of the silica nanofibres in Tris-buffer (pH 8.5), the as-prepared SiO_2@PDA core-shell nanostructure was carbonised at high temperature in an inert gas to prepare the SiO_2@C nanostructure. Finally, the Si nanoparticles' encapsulation into each carbon nanotube was achieved by an in-situ magnesiothermic reduction. The products obtained were black (Figure S1c). Experimental methods and details of all materials used are described in the Experimental Section.

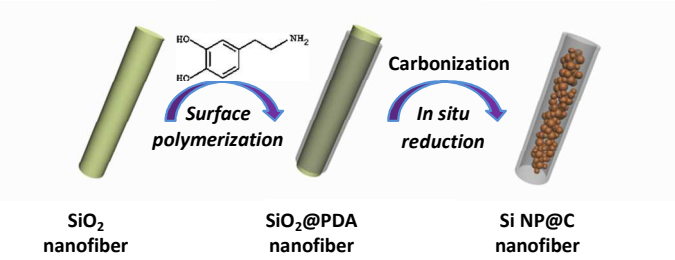

Figure 1. Schematic illustration of the preparation of the Si NP@C core-shell nanofibres.

The morphology of the bare SiO_2 nanofibres and Si nanofibres was characterised by scanning electron microscopy (SEM) and transmission electron microscopy (TEM), respectively. A panoramic view of the as-fabricated SiO_2 and Si showed that the nanofibres were uniform with a diameter of approximately 500 nm (Figure S2). TEM investigation has been carried out for better visualisation of the nanostructure. Figure S2c and d show the bare Si nanofibres without any carbon coating. It demonstrated that the Si nanofibres were composed of Si nanoparticles with an average particle size of approximately 10 nm. The structure of the SiO_2@C nanofibres and Si NP@C core-shell nanofibres were first characterised by SEM and TEM. The samples synthesised from the electro-spinning and magnesiothermic reduction steps revealed a 1D fibrous morphology with an average diameter of approximately 500 nm and several tens of microns in length. Figure 2c and d show the morphology of the Si NP@C nanofibres: they had a smooth surface. With a further increase in magnification, a SEM cross-section of a single Si NP@C nanofibre shows that Si NPs were well-confined within the core section (inset to Figure 2c). The TEM images of Si NP@C nanofibres (Figure 2d) indicated that Si NPs were indeed encapsulated in the carbon fibres, forming a core-shell

Nanoscale Accepted Manuscript

This journal is © The Royal Society of Chemistry [year]

nanostructure. The thickness of the carbon layer was found to be approximately 20 nm and the particle size of Si NP in the carbon nanofibers is around 10 nm (Figure S3). The abundant void space surrounding each Si nanoparticle can also be observed which permitted the Si to expand without mechanical constraint during lithiation and also prevented damage to the carbon layer therefrom. From the well-resolved lattice fringes of the high-resolution TEM (HRTEM) image (Figure 2e) taken from the edge of one nanofibre, an interplanar spacing of 0.31 nm was obtained, that being consistent with the distance of the (111) plane of the Si. This result suggested that the Si NP confined in carbon nanofibres was crystalline. To inquire further into the distribution of the Si NPs in the carbon nanofibres, TEM-energy dispersed spectroscopy (EDS) was carried out, as seen in Figure 2f and g. Along the nanofibres, Si and C were uniformly distributed on the whole nanofibres: this further indicated the formation of Si NP@C core-shell nanofibres.

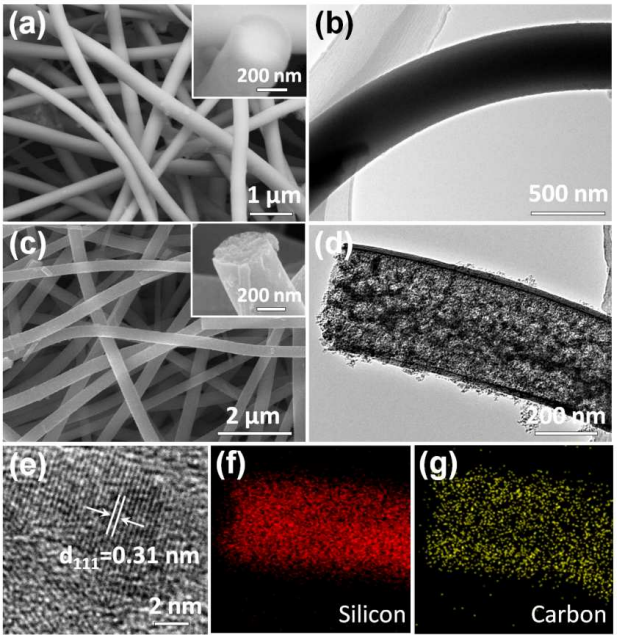

Figure 2. (a, b) SEM and TEM images of SiO_2@C nanofibres. (c, d) SEM and TEM images Si NP@C nanofibres. (e) HRTEM images of Si NP@C nanofibres. (f, g) EDS mapping images of Si (red), C (yellow).

The phase structure and composition of these samples were determined by X-ray diffraction (XRD). The XRD pattern of the SiO_2 nanofibres (Figure S4) shows a single broad peak centered between 20° and 30°, which meant that the samples had an amorphous structure. Figure 3a shows the XRD pattern of the SiO_2@C after magnesiothermic reduction, the major identified peaks at 28.5°, 47.2°, 56.2°, 69.2°, and 76.3°, were indexed as the (111), (220), (311), (400), and (331) planes of the cubic diamond phase of silicon (JCPDS 27-1402), respectively. No other characteristic peaks arising from impurities were observed, indicating the effective transformation of SiO_2 into Si by this magnesiothermic reduction process. The same peaks were also observed in the bare Si sample (Figure S3). The porous structure and surface area were studied by N_2 adsorption–desorption measurement on samples of Si NP@C nanofibres (Figure 3b). From the isotherm, the samples exhibited hysteresis in the high relative pressure region, indicating the existence of meso- and micro-porous. According to test reports, the Si NP@C nanofibres had a surface area of 263.05 m^2 g^{-1}. The relatively high surface area of the composite was significant as it allowed active materials to participate in the reaction and a large particle-electrolyte interface ensured that the Si nanoparticles participated in the ultra-fast electrochemical reaction. The pore-size distribution calculated by the Barrett-Joyner-Halenda (BJH) method, based on the desorption branch of the isotherms, indicated that the composite had a mesopore size of 7.3 nm. The mesopores formed in the silicon nanofibres were attributed to the removal of the template and the volume occupied by the magnesium oxide formed by magnesiothermal reduction. The ample pore structure in the composite may be favourable to accessing the electrolyte solution and to accommodating the volume changes of the Si nanoparticles during charge-discharge cycles.

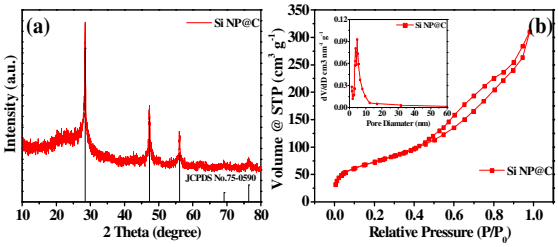

Figure 3. (a) XRD patterns of Si NP@C nanofibres. (b) A nitrogen adsorption-desorption isotherm for the Si NP@C nanofibres. Inset: pore size distribution of Si NP@C nanofibres.

The composites were then assembled into Li half-cells to evaluate the effects of the core-shell nanofibre structure on electrochemical performance. For comparison, bare Si nanofibres were also synthesised and tested. The specific capacity values were based on the total weight of Si NP@C nanofibres: the carbon comprised approximately 11.7% of the mass, as evaluated by thermo-gravimetric analysis (TGA, Figure S5). Figure 4a shows the charge-discharge profiles of bare Si nanofibres at a current density of 0.1 A g^{-1} within a voltage window between 0.01 and 1.5 V. A distinct plateau profile at 0.1 to 0.01 V was seen, indicating that the lithium had alloyed with crystalline Si nanoparticles. It was reported that the alloying process in Si anodes leads to the formation of $Li_{12}Si_7$, $Li_{14}Si_6$, $Li_{13}Si_4$, and eventually a $Li_{22}Si_5$ alloy.[33, 34] Upon the following Si charging process, a plateau at about 0.4 V could be observed. The first discharge and charge capacities of bare Si were 1762.3 and 892.3 mA h g–1, respectively, the Coulombic efficiency (CE) was 50.6%. The relatively low initial CE of bare Si nanofibres can be ascribed to the pulverization and disruption of the microstructure of the electrode, which in turn resulted in a large irreversible capacity. Upon cycling, the voltage profiles showed gradual capacity fade, yielding a large reduction in the capacities. It was noted that, when the same experimental protocols were repeated with the Si NP@C nanofibre samples, distinctly different cycling behaviour resulted (Figure 4b). In addition to the potential plateau at 0.1 V, steps were observed at 1.2 V and 0.80 to 0.20 V, which demonstrated SEI formation by irreversible reduction of electrolyte on the surface of the carbon shell. The initial

Nanoscale Accepted Manuscript

discharge/charge capacity of Si NP@C was 2359.7/1049.5 mAh g^{-1}, corresponding to a CE of 44.5%. The observed large irreversible capacity in the first cycle may be ascribed to the relatively low quality of the carbon layer and the initial SEI formation expending some of the electrolyte. Besides that, the significantly increased surface area may consume more lithium ions and thus bringing about a remarkable decrease of the first CE. The CE can be augmented by graphitisation and pre-lithiation of carbon fibres in future studies.[35, 36] However, after the first cycle, the shape of the charge/discharge profiles almost overlapped upon cycling, implying good stability of the electrode, which can benefit from the better electric conductivity of carbon fibre and the volume buffer effect of the pore structure.

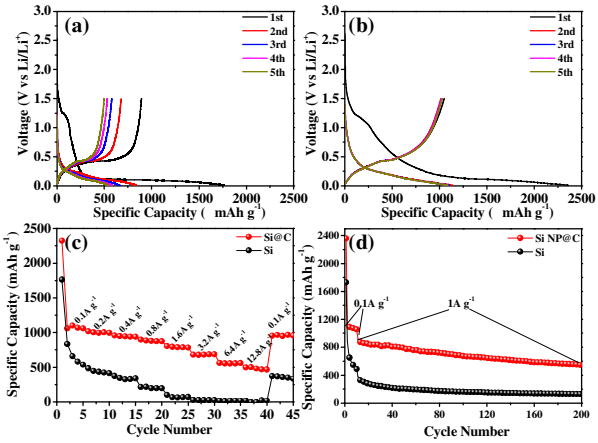

Figure 4. Charge/discharge profiles of (a) pure Si nanofibres and (b) Si NP@C nanofibres at a current density of 0.1 A g^{-1}. (c) Rate capability tests for Si NP@C nanofibres and pure Si nanofibres at various C-rates. (d) Cycling performance of Si NP@C nanofibres and pure Si nanofibres measured at 1 A g^{-1}.

The Si NP@C nanofibres also had a much better rate performance than the bare Si nanofibres, as shown in Figure 4c. The assembled cell, using composites as its active materials, was first tested at the same charge and discharge current densities of 0.1 A g^{-1}, and then at increased current densities from 0.2 A g^{-1} to 12.8 A g^{-1}. The composites delivered a high average capacity of 1071.5 mA h g^{-1} at 0.1 A g^{-1}. When the cycle rate was changed from 0.1 A g^{-1} to 0.8 A g^{-1}, a small decrease in discharge capacity from 1071.5 to 874 mAh g^{-1} was observed. Apparently, Li^+ passed rapidly through the thin carbon layer and reacted with the Si nanoparticles within even at very high current densities. With an increased current density, the capacity decreased slightly. Upon further increases to a current density of 12.8 A g^{-1}, a high capacity of 466.8 mAh g^{-1} could still be obtained, which was higher than the theoretical capacity of graphite (372 mAh g^{-1}). When the cycle rate was reduced to 0.1 A g^{-1} after 40 cycles at different current densities, the charge capacity increased again to 957.4 mAh g^{-1}, corresponding to 89.3% of the initial capacity obtained at 0.1 A g^{-1}. In contrast, the bare Si nanofibres exhibited lower average capacities of 652.1 mAh g^{-1} at 0.1 A g^{-1}, with a poorer rate capability (their capacity was 18.6 mAh g^{-1} at 12.8 A g^{-1}): most importantly, the LIB rate performance of Si NP@C nanofibres was greatly enhanced compared to that previously reported for Si@C nanowires, [37] mpSi@void@mpC[38, 39] and even many graphene-based, Si-based materials[40, 41]. This can be ascribed to the strong synergistic effect between the Si core and the carbon shell. In the Si NP@C nanofibres, all of the Si NPs adhered onto the inner surface of the carbon nanofibres, leading to a large contact surface area with good adherence. This helped to build good electrical contact with the conducting carbon, and the empty space can accommodate the volume changes during charge-discharge cycles. Figure 4d shows the cycling stability of Si nanofibres and Si NP@C nanofibre electrodes during charging and discharging in the range 0.01 to 1.5 V (vs Li/Li^+ ratio) at 1 A g^{-1}. Under deep charge/discharge conditions, the pure Si nanofibres without carbon coatings had a fast capacity fade from an initial 1728.9 mAh g^{-1} to 127.6 mAh g^{-1} after 200 cycles. This was because the disconnection between Si nanoparticles and the current collector, and the volume expansion/contraction caused the continuous formation of an SEI layer which isolated the active materials. In comparison, the core-shell Si NP@C nanofibres demonstrated excellent discharge capacity retention during cycling. The capacity of Si NP@C nanofibres retained a specific discharge capacity of 546.9 mAh g^{-1} after 200 cycles and the corresponding Coulombic efficiency was shown in the Figure S6. To further confirm the cycling stability, the cycle performance of Si NP@C nanofibers for 50 cycles at 0.1 A g^{-1} is also given in Figure S7. After 50 cycles, the capacity of Si NP@C nanofibers retained a specific discharge capacity of 908.5 mAh g^{-1} which proved their superior cycling stability. EIS technique is also utilized to clarify the remarkable electrochemical performance of Si NP@C nanofibres compared with Si nanofibres (Figure S8). The charge-transfer resistance (Rct) parameters of the bare Si electrodes are obviously lager than that of the Si NP@C composite electrode after the 200 cycles at rate of 1 A g^{-1},which indicates it has higher electrical conductivity than that of the bare Si electrodes. This difference may be due to the uniform carbon shell maintains their structural integrity and enchance the electronic conductivity of the whole electrode. We believed that this improved electrochemical performance of the composite electrode mainly resulted from its unique structure. The composite material contained plentiful void spaces around each Si nanoparticle, which were generated during the in situ reduction process, and were conducive to the effective accommodation of significant volumetric expansion and the protection of structure and morphology. Whereas the carbon shell enabled fast electron transmission for the Si nanoparticles, as a protective layer avoided exposure of any Si nanoparticles to electrolytic decomposition. In addition, the carbon shell could effectively limit the formation of SEI during the initial charge-discharge process.

Nanoscale Accepted Manuscript

This journal is © The Royal Society of Chemistry [year]

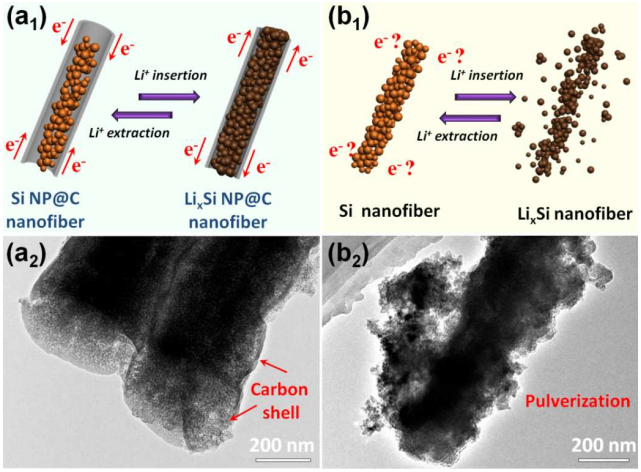

Figure 5. (a_1, b_1) Schematic illustration of electrode morphology change, (a_2, b_2) TEM images of Si NP@C nanofibre composite after 200 cycles and the bare Si nanofibre after 50 cycles at a current density of 1 A g^{-1}.

To confirm that the Si NP@C nanofibre electrode can still retain robust mechanical properties after cycling, TEM images of the electrodes were collected after cycling to analyse any changes in structure or morphology in the active material. As shown in Figure 5a, after over 200 cycles, from the TEM image of the Si NP@C nanofibres, the silicon expanded inside the carbon framework to occupy the void spaces, resulting in little change to both the carbon shell and secondary particle size. In view of the protection offered by the carbon shell, the expansion in the radial direction was not remarkable. Therefore, the Si NP@C nanofibre morphology could be well-maintained during charging-discharging cycles. In Figure S9 also show the TEM image of Si NP@C nanofibers after 200 cycles at 1 A g^{-1} and corresponding EDS mapping images. On the contrary, the bare Si nanofibre, after 50 cycles under the same test conditions, suffered broken nanofibres and pulverisation of Si nanoparticles (Figure 5b). This turned out to be direct proof of the structural stability of Si NP@C nanofibres and it was important with regard to the exceptional electrochemical lithium storage capability.

Conclusions

In summary, the Si NPs confined within carbon fibres have been successfully fabricated through a self-polymerisation of dopamine on the surface of SiO_2 nanofibres, and the subsequent carbonisation of PDA, combined with the in situ reduction of the core material. The Si NP@C nanofibres exhibited high reversible capacity, excellent rate capability, and good cycling performance. The enhanced electrochemical properties could be attributed to the interpenetrating network of carbon nanofibres and their provision of high conductivity, good mechanical properties, facile ion transport, and the in situ formation of sufficient empty space, thus leading to facile electrode kinetics and high strain tolerance during volumetric changes. The scalable, novel, nanostructural material designed here is not only a good model for highly reversible silicon composite anodes, but can also be readily applied to other LIB electrode materials that suffer from volume changes.

Acknowledgements

This work was supported by the National Basic Research Program of China (973 Program) (No. 2014CB239701), National Natural Science Foundation of China (No. 21173120, 51372116), Natural Science Foundation of Jiangsu Province (BK2011030, BK2011740), the Fundamental Research Funds for the Central Universities of NUAA (NP2014403) and a Project Funded by the Priority Academic Program Development of Jiangsu Higher Education Institutions (PAPD).

Notes and references

Jiangsu Key Laboratory of Materials and Technology for Energy Conversion, College of Material Science and Engineering, Nanjing University of Aeronautics and Astronautics, Nanjing, 210016, P.R. China
Corresponding author Tel: +86 025 52112902; Fax: +86 025 52112626.
E-mail address: azhangxg@nuaa.edu.cn

† Electronic Supplementary Information (ESI) available: [details of any supplementary information available should be included here]. See DOI: 10.1039/b000000x/

1. M. Armand and J. M. Tarascon, *Nature*, 2008, **451**, 652-657.
2. M. S. Whittingham, *Chemical Reviews*, 2004, **104**, 4271-4301.
3. J. R. Szczech and S. Jin, *Energy & Environmental Science*, 2011, **4**, 56-72.
4. J. B. Goodenough and Y. Kim, *Chemistry of Materials*, 2010, **22**, 587-603.
5. R. A. Huggins, *Journal of Power Sources*, 1999, **81**, 13-19.
6. U. Kasavajjula, C. Wang and A. J. Appleby, *Journal of Power Sources*, 2007, **163**, 1003-1039.
7. C. K. Chan, H. Peng, G. Liu, K. McIlwrath, X. F. Zhang, R. A. Huggins and Y. Cui, *Nature Nanotechnology*, 2008, **3**, 31-35.
8. T. D. Hatchard and J. R. Dahn, *Journal of the Electrochemical Society*, 2004, **151**, A838-A842.
9. T. H. Hwang, Y. M. Lee, B.-S. Kong, J.-S. Seo and J. W. Choi, *Nano Letters*, 2012, **12**, 802-807.
10. M. Gauthier, D. Mazouzi, D. Reyter, B. Lestriez, P. Moreau, D. Guyomard and L. Roue, *Energy & Environmental Science*, 2013, **6**, 2145-2155.
11. S. R. Gowda, V. Pushparaj, S. Herle, G. Girishkumar, J. G. Gordon, H. Gullapalli, X. Zhan, P. M. Ajayan and A. L. M. Reddy, *Nano Letters*, 2012, **12**, 6060-6065.
12. N. Binh Phuong Nhan, N. A. Kumar, J. Gaubicher, F. Duclairoir, T. Brousse, O. Crosnier, L. Dubois, G. Bidan, D. Guyomard and B. Lestriez, *Advanced Energy Materials*, 2013, **3**, 1351-1357.
13. G. Kim, S. Jeong, J.-H. Shin, J. Cho and H. Lee, *ACS Nano*, 2014, **8**, 1907-1912.
14. Y. Yu, L. Gu, C. B. Zhu, S. Tsukimoto, P. van Aken, and J. Maier, *Advanced Materials*, 2010, **22**, 2247-2250.
15. K. Evanoff, J. Benson, M. Schauer, I. Kovalenko, D. Lashmore, W. J. Ready and G. Yushin, *ACS Nano*, 2012, **6**, 9837-9845.
16. W. J. Lee, T. H. Hwang, J. O. Hwang, H. W. Kim, J. Lim, H. Y. Jeong, J. Shim, T. H. Han, J. Y. Kim, J. W. Choi and S. O. Kim, *Energy & Environmental Science*, 2014, **7**, 621-626.
17. H. Jiang, Y. Hu, S. Guo, C. Yan, P. S. Lee and C. Li, *Acs Nano*, 2014, **8**, 6038-6046.
18. S. Fang, L. Shen, G. Xu, P. Nie, J. Wang, H. Dou and X. Zhang, *ACS Applied Materials & Interfaces*, 2014, **6**, 6497-6503.
19. B. S. Lee, H. S. Yang, H. Jung, S. Y. Jeon, C. Jung, S. W. Kim, J. Bae, C. L. Choong, J. Im, U. I. Chung, J. J. Park and W. R. Yu, *Nanoscale*, 2014, **6**, 5989-5998.
20. B. Wang, X. Li, X. Zhang, B. Luo, Y. Zhang and L. Zhi, *Advanced Materials*, 2013, **25**, 3560-3565.
21. H. Wu, G. Chan, J. W. Choi, I. Ryu, Y. Yao, M. T. McDowell, S. W. Lee, A. Jackson, Y. Yang, L. Hu and Y. Cui, *Nature Nanotechnology*, 2012, **7**, 309-314.
22. B. Hertzberg, A. Alexeev and G. Yushin, *Journal of the American Chemical Society*, 2010, **132**, 8548-8549.

Nanoscale Accepted Manuscript

23. J. Deng, H. Ji, C. Yan, J. Zhang, W. Si, S. Baunack, S. Oswald, Y. Mei and O. G. Schmidt, *Angewandte Chemie-International Edition*, 2013, **52**, 2326-2330.
24. N. Liu, H. Wu, M. T. McDowell, Y. Yao, C. Wang and Y. Cui, *Nano Letters*, 2012, **12**, 3315-3321.
25. Y. Park, N. S. Choi, S. Park, S. H. Woo, S. Sim, B. Y. Jang, S. M. Oh, S. Park, J. Cho and K. T. Lee, *Advanced Energy Materials*, 2013, **3**, 206-212.
26. J. Q. Wang, Y. Yu, L. Gu, C. L. Wang, K. Tang and J. Maier, *Nanoscale*, 2013, **5**, 2647-2650.
27. S. Cavaliere, S. Subianto, I. Savych, D. J. Jones and J. Roziere, *Energy & Environmental Science*, 2011, **4**, 4761-4785.
28. M. Inagaki, Y. Yang and F. Kang, *Advanced Materials*, 2012, **24**, 2547-2566.
29. L. Ji, Z. Lin, B. Guo, A. J. Medford and X. Zhang, *Chemistry-a European Journal*, 2010, **16**, 11543-11548.
30. H. Wu, G. Zheng, N. Liu, T. J. Carney, Y. Yang and Y. Cui, *Nano Letters*, 2012, **12**, 904-909.
31. X. Zhou, L. J. Wan and Y. G. Guo, *Small*, 2013, **9**, 2684-2688.
32. K. Fu, Y. Lu, M. Dirican, C. Chen, M. Yanilmaz, Q. Shi, P. D. Bradford and X. Zhang, *Nanoscale*, 2014, **6**, 7489-7495.
33. M. Zeilinger, I. M. Kurylyshyn, U. Haussermann and T. F. Faessler, *Chemistry of Materials*, 2013, **25**, 4623-4632.
34. M. T. McDowell, I. Ryu, S. W. Lee, C. Wang, W. D. Nix and Y. Cui, *Advanced Materials*, 2012, **24**, 6034-6041.
35. C. Kim, K. S. Yang, M. Kojima, K. Yoshida, Y. J. Kim, Y. A. Kim and M. Endo, *Advanced Functional Materials*, 2006, **16**, 2393-2397.
36. J. K. Lee, K. W. An, J. B. Ju, B. W. Cho, W. I. Cho, D. Park and K. S. Yun, *Carbon*, 2001, **39**, 1299-1305.
37. J. K. Yoo, J. Kim, H. Lee, J. Choi, M. J. Choi, D. M. Sim, Y. S. Jung and K. Kang, *Nanotechnology*, 2013, **24**.
38. Y. Ru, D. G. Evans, H. Zhu and W. Yang, *Rsc Advances*, 2014, **4**, 71-75.
39. Y. Ma, G. Ji, B. Ding and J. Y. Lee, *Journal of Materials Chemistry A*, 2013, **1**, 13625-13631.
40. H. Tang, J. P. Tu, X. Y. Liu, Y. J. Zhang, S. Huang, W. Z. Li, X. L. Wang and C. D. Gu, *Journal of Materials Chemistry A*, 2014, **2**, 5834-5840.
41. C. Ma, C. Ma, J. Wang, H. Wang, J. Shi, Y. Song, Q. Guo and L. Liu, *Carbon*, 2014, **72**, 38-46.

Si Nanoparticles Encapsulated in Elastic Hollow Carbon Fibre for Li-Ion Battery Anodes with High Structure Stability

*Shan Fang, Laifa Shen, Zhenkun Tong, Hao Zheng, Fang Zhang, Xiaogang Zhang**

Here, a novel one-dimensional core-shell nanostructure in which the Si nanoparticles have been confined within hollow carbon nanofibres. Such a unique nanostructures exhibits high conductivity, facile ion transport, and the uniform pores within the particles which are generated during magnesiothermic reduction can serve as a buffer zone to accommodate the large volume changes of Si during electrochemical lithiation. The hierarchical nanostructures show superior rate capabilities and stable cycling performance in rechargeable batteries.

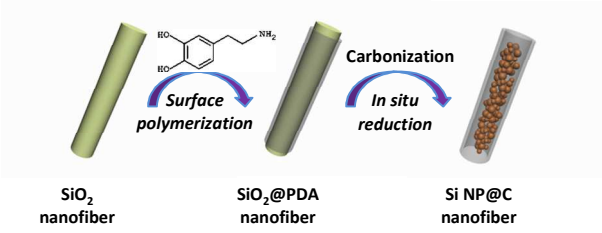

Nanoscale Accepted Manuscript

This journal is © The Royal Society of Chemistry [year]